JOURNAL OF Applied Polymer SCIENCE

Transparent, Flexible, and High-Strength Regenerated Cellulose/Saponite Nanocomposite Films with High Gas Barrier Properties

Quanling Yang, Tsuguyuki Saito, Akira Isogai
Department of Biomaterial Sciences, Graduate School of Agricultural and Life Sciences, The University of Tokyo, 1-1-1 Yayoi, Bunkyo-Ku, Tokyo 113-8657, Japan
Correspondence to: A. Isogai (E-mail: aisogai@mail.ecc.u-tokyo.ac.jp)

ABSTRACT: Regenerated cellulose-saponite nanocomposite films were prepared from LiOH/urea solutions, and exhibited high optical transparency and flexibility. The saponite platelets formed intercalated nanolayered structures in the composites. The longitudinal directions of both the cellulose II crystallites and the saponite platelets were preferentially oriented parallel to the film surface in the composites. The good nanodispersibility and high orientation of the saponite platelets in the composite films resulted in high mechanical strength, high Young's modulus, and good thermal dimensional stabilities, and gas barrier properties in the composites, compared with a reference cellulose film. Moreover, the tensile strength and Young's modulus of the composite film reached 241 MPa and 7.7 GPa, respectively, when a simple drawing process was applied to the wet composite film; this is probably owing to the improvement in the orientation of the cellulose II crystallites and saponite platelets in the composites. The composite films also showed high toughness and ductility. © 2013 Wiley Periodicals, Inc. J. Appl. Polym. Sci. 000: 000–000, 2013

KEYWORDS: cellulose and other wood products; composites; X-ray; mechanical properties

Received 6 March 2013; accepted 16 May 2013; Published online 00 Month 2013
DOI: 10.1002/app.39564

INTRODUCTION

Highly transparent, flexible, and low-cost thin gas barrier films are in great demand for the packaging of food and medicine, the encapsulation of electronic devices, and for flexible organic light-emitting diode (OLED) displays.[1,2] The lack of a practical barrier layer is the primary hurdle faced by the flexible electronics industry.[3] Petroleum-based synthetic polymers such as poly(vinylidene chloride), ethylene vinyl alcohol copolymers, nylon, and polymers with vapor-deposited coatings have been used as gas barrier films for these purposes.[4] However, polymers with vapor-deposited coatings are prone to cracking when they are folded, and additional fabrication processes are therefore needed for such materials.[5,6] Most of the synthetic polymers used in our daily lives are non-renewable and cause environmental pollution, because they are not biodegradable or carbon neutral.[7] Therefore, the development of new renewable, biodegradable, and biocompatible bio-based gas-barrier materials is a requirement for a sustainable society.[8]

Cellulose is the most abundant natural polymer, and has potential as a renewable resource for applications in versatile commodity and high-tech materials.[9] Because cellulose is not a thermo-plastic material, it must be dissolved in a solvent and regenerated from the cellulose solution in a non-solvent system (this process is known as wet forming) for it to be formed into films, fibers, hollow fibers, or other morphologies that confer some functionality on cellulose. However, native celluloses are typically difficult to dissolve in common solvents, due to the presence of highly regulated and numerous inter- and intramolecular hydrogen bonds, which restrict its potential applications in forming processes. New solvents for cellulose have been developed in recent decades, including N-methylmorpholine-N-oxide hydrate,[10,11] ionic liquids,[12,13] and aqueous alkali/urea solutions.[14–16]

In the previous work, regenerated cellulose films prepared from aqueous alkali/urea solutions were found to exhibit good optical transparency, biocompatibility, biodegradability, and oxygen barrier properties under dry conditions.[17–21] Moreover, the mechanical properties, thermal dimensional stability, and oxygen barrier properties of the cellulose films were improved via compositing with natural montmorillonite clay (MTM).[22] The formation of intercalated nanolayered MTM platelets structures in the cellulose matrix was likely responsible for these improvements in the film properties.[23–27] However, the planes of the MTM platelets are large, and not uniform. In addition, the optical transmittance of the cellulose-MTM composite films clearly decreased as the MTM content was increased, probably due to the increased aggregation of the MTM platelets in the composites. Recently, commercially available synthetic smectite

saponite (SPN) clays were used as nanofillers to prepare clay-polymer composites, which had not only good mechanical, thermal, and oxygen barrier properties, but also high optical transparency; the good optical properties resulted from the fact that the synthetic saponite clays have higher-purity and smaller and more uniform planes than MTM.[1]

In this work, regenerated cellulose films fabricated from LiOH/urea/cellulose (LUC) solutions were reinforced with SPN platelets to improve their mechanical, thermal, and gas barrier properties and maintain their good optical transparency. Compared with other newly developed cellulose solvents like ionic liquids,[12,13] aqueous alkali/urea systems are thought to have great economic and environmental advantages.[14] Moreover, the aqueous LiOH/urea system is more powerful than the similar aqueous NaOH/urea system, in terms of dissolution of celluloses with higher molecular weights and preparation of cellulose solutions with higher cellulose concentrations. The orientation behavior of the SPN platelets and cellulose II crystallites in the composite films, and the relationships between the SPN structures in the cellulose matrix and the properties of the composites were studied. Moreover, differences in the structures and properties of composite films containing SPN and MTM as nanofillers were investigated. The effects of film drawing on the mechanical properties of the composite films were also investigated.

EXPERIMENTAL

Materials

A filter paper pulp (highly purified cotton linters, Advantec, Tokyo, Japan) was used as the cellulose sample; the sample had a viscosity-average molecular weight of 8.6×10^4 g mol^{-1}.[22] A commercially available synthetic smectite saponite (SPN) with an aspect ratio of 50 (Smecton SA) was supplied by Kunimine Industries, Japan. The chemical formulae of the SPN is $Na_{1/3}Mg_3(Si_{11/3}Al_{1/3})O_{10}(OH)_2$, according to the manufacturer data. All reagents and solvents were of laboratory grade, were used as received, and were obtained from Wako Pure Chemicals, Tokyo, Japan.

Film Preparation

The cellulose solvent was prepared as a mixed solution of LiOH/urea/H_2O (4.6:15:80.4, by weight). A desired amount of SPN was dispersed in the above solvent and then stirred for 2 h at room temperature. The SPN dispersion was further agitated at 7500 rpm for 2 min at room temperature using a double-cylinder-type homogenizer (Excel Auto ED-4, Nissei, Japan), and was then sonicated for 6 min using an ultrasonic homogenizer with a 26 mm-diameter probe tip, at an output power of 300 W (US-300T, Nissei, Japan). The SPN dispersion thus obtained was then cooled to −12°C in a refrigerator. A desired amount of cellulose was dispersed in the cooled SPN dispersion, which was then stirred immediately at 1200 rpm for 10 min to obtain a transparent solution with cellulose content of 4 wt %. The blend solution was degassed via centrifugation at $5600 \times g$ for 10 min, spread on a glass plate as a 0.5 mm-thick layer, and then immersed in acetone at room temperature for 30 min, to allow regeneration to occur. The resulting sheet-like hydrogels were thoroughly washed with water via repeated soaking treatment, fixed on a poly(methyl methacrylate) plate with adhesive tape to prevent shrinkage, and then air-dried at ambient temperature to obtain the composite films. The weight ratios of cellulose and SPN in the composite films were 100:0, 95:5, 90:10, 85:15, and 80:20, which are abbreviated here as LUC, LUC-SPN5, LUC-SPN10, LUC-SPN15, and LUC-SPN20, respectively. To study the effects of drawing, the wet film (LUC-SPN15) was drawn and dried at a draw ratio of 1.15 for 8 h, using a tensile testing apparatus (Shimadzu EZ-TEST) at room temperature. The obtained drawn film is denoted here as LUC-SPN15D.

A desired amount of SPN was dispersed in deionized water, and the dispersion was stirred and agitated as described above to prepare a 2 wt % SPN/water dispersion. The obtained SPN dispersion was dried in a ventilated oven at 40°C for 3 days to obtain a SPN film. The SPN was dispersed in a 4.6 wt % LiOH solution and then washed thoroughly with water via repeated centrifugation, to prepare SPN with Li^+ ions in place of Na^+ ions. The SPN film with Li ions that was prepared using the procedure described above is named there as Li-SPN.

Characterization

Wide-angle X-ray diffraction (WAXD) patterns of the films were acquired in reflection mode, using a RINT 2000 diffractometer (Rigaku, Tokyo, Japan) with monochromator-filtered Cu Kα radiation.[22] Two-dimensional X-ray diffraction patterns (2D XRD) were obtained at room temperature using nickel-filtered Cu Kα radiation with a wavelength of 0.15418 nm, which was generated using a rotating anode X-ray generator (Rigaku RU-200BH) operating at 50 kV and 100 mA. The X-ray beam was applied to the film surface plane or film cross-section. The patterns were recorded on flat-plate imaging plates (Fuji Film BAS-IP SR 127) using an evacuated camera. Sodium fluoride ($d = 0.23166$ nm) was dusted on the surface of the samples to provide a calibration. From the azimuthal intensity distribution graphs for the (1−1 0) reflection of cellulose II or the (0 0 1) reflection of SPN, two orientation factors—the degree of orientation (Π), and Herman's orientation parameter (f)—were calculated according to a previously reported method.[28]

The LUC and LUC-SPN composite films were frozen in liquid nitrogen, immediately snapped, and then vacuum-dried. The surfaces and cross-sections were observed using a Hitachi S4800 field-emission scanning electron microscope (SEM), after osmium coating. Energy-dispersive X-ray (EDX) analysis of the SPN and the LUC-SPN composite films was carried out using a Horiba EMAX Energy spectroscope attached to the SEM.

The optical transmittance of the films was measured from 400 to 800 nm using a JASCO V-670 UV-Vis spectrophotometer. Tensile tests were performed using a Shimadzu EZ-TEST instrument equipped with a 500 N load cell. Rectangular strips 2×30 mm^2 in size were cut from the films and tested with a span length of 10 mm, at a rate of 1.0 mm min^{-1}. At least 10 measurements were carried out for each sample. In the case of the LUA-SPN15D film, the tensile test was carried out to the film direction parallel to that of drawing. The thermal expansion of the films was determined (following preheating at 120°C

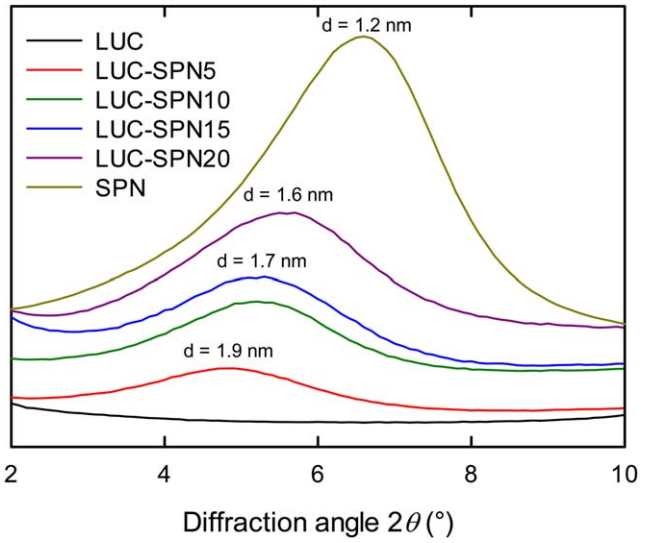

Figure 1. WAXD patterns for LUC, SPN, and LUC-SPN composite films. [Color figure can be viewed in the online issue, which is available at wileyonlinelibrary.com.]

for 10 min) using a Shimadzu TMA-60 thermomechanical analyzer under a load of 0.03 N, in a nitrogen atmosphere, with temperatures from 28 to 100°C, and a heating rate of 5°C min^{-1}.

The rates of oxygen and water vapor transmission in the films were determined using Mocon Ox-Tran Model 2/21MH and Mocon Permatran-W Model 1/50G (Modern Controls, USA) instruments, respectively, under standard conditions (ASTM 3985). The gas permeability was calculated from the gas transmission rate and the film thickness, and the standard deviations for each film were within ±5%. The thicknesses of the films (~30 μm) were measured using a micrometer, and were expressed as an average of five measurements, with statistical errors within 3%. The moisture contents and water-uptake values of the films were measured according to previously reported methods.[22]

RESULTS AND DISCUSSION

Structures of Cellulose-Saponite Composite Films

The WAXD patterns for the LUC, SPN, and LUC-SPN composite films are shown in Figure 1. The *d*-spacing of the (0 0 1) plane of SPN was calculated to be 1.2 nm from the diffraction peak at $2\theta = 6.6°$, using the Bragg equation; this value was the same as that of natural MTM clay.[22] The *d*-spacing of SPN increased from 1.2 to 1.9 nm in the LUC-SPN composite films as the cellulose content was increased from 0 to 95 wt %, which indicated the formation of intercalated SPN platelet structures in the cellulose matrix. The (0 0 1) *d*-spacings of the LUC-SPN composite films were larger than those of the LUC-MTM composite films (1.6 nm), indicating the higher intercalation efficiency of the SPN platelets compared with the MTM platelets. The *d*-spacing of 1.6 nm for SPN in the LUC-SPN20 film was 0.4 nm larger than that measure for the neat SPN film (1.2 nm) due to the presence of a single layer (ca., 0.4 nm) of cellulose molecules between the SPN platelets. The *d*-spacing of SPN in the LUC-SPN5 film increased to 1.9 nm due to the presence of a double layer of cellulose molecules between the SPN platelets.

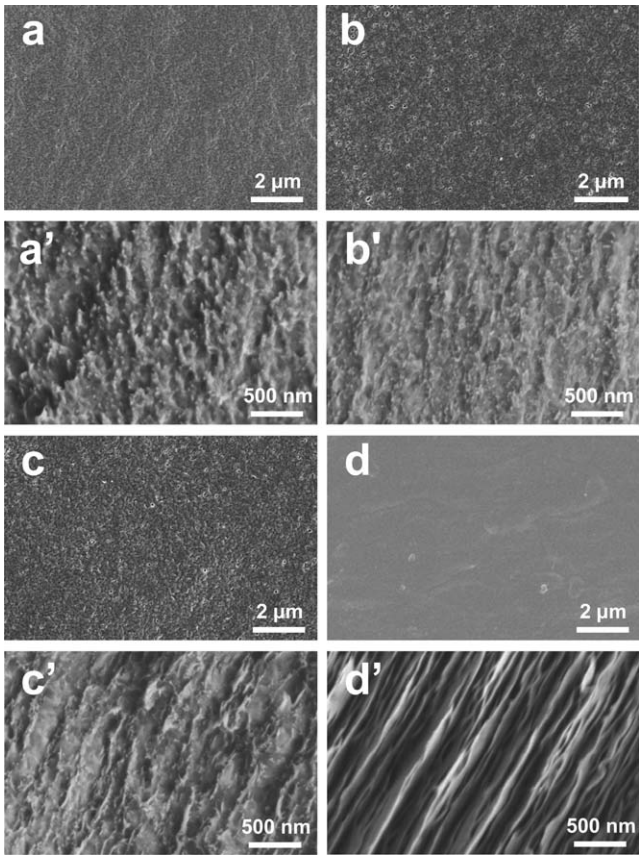

Figure 2. SEM images of the surfaces of LUC (a), LUC-SPN5 (b), LUC-SPN15 (c), and SPN (d) films, and those of cross-sections of LUC (a'), LUC-SPN5 (b'), LUC-SPN15 (c'), and SPN (d') films.

SEM images of the surfaces and cross-sections of the LUC, LUC-SPN5, LUC-SPN15, and SPN films are shown in Figure 2. The surfaces of the composite films were uniform, indicating good compatibility between the cellulose and SPN in the composites. As shown in the SEM image of the SPN film cross-section, the SPN platelets formed regular and nanolayered structures. Similar nanolayered structures were observed in the cross-sections of the LUC-SPN composite films with high SPN contents. Meanwhile, the SPN platelets became thinner and displayed smaller interstices as the cellulose content in the composite was increased. The WAXD and SEM results indicated the formation of intercalated and nanolayered SPN platelet structures in the cellulose matrix.[1,22–27,29]

The orientation behavior of the SPN platelets and cellulose II crystallites in the LUC-SPN15 and LUC-SPN15D composite films was studied using 2D XRD (Figure 3). Ring diffractions indicate the random orientation of crystallites, whereas arc diffractions are characteristic of their preferred orientations. The cellulose II crystallites and the SPN platelets were randomly oriented in the film plane direction in both the LUC-SPN15 and LUC-SPN15D composite films. In contrast, clear diffraction arcs were observed for both SPN and cellulose II when X-ray

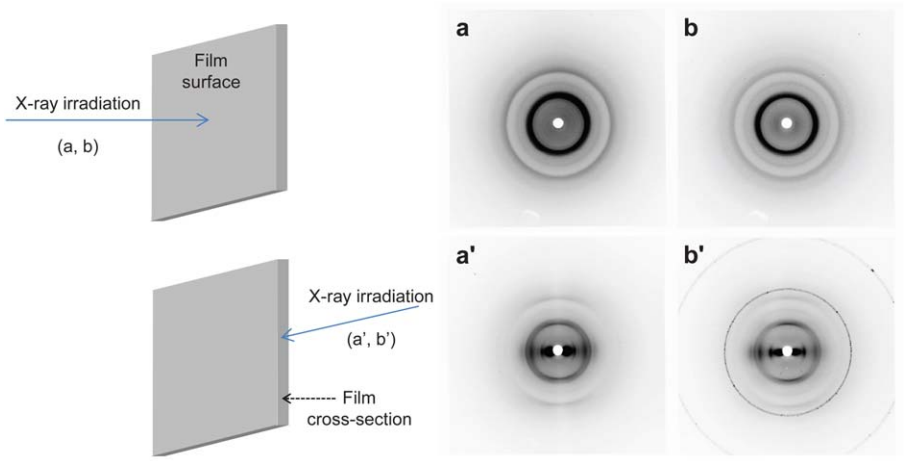

Figure 3. Two-dimensional XRD diagrams for LUC-SPN15 (a, a') and LUC-SPN15D (b, b') films. The X-ray beam was applied perpendicular (a, b), and parallel (a', b') to the film surface plane, respectively. [Color figure can be viewed in the online issue, which is available at wileyonlinelibrary.com.]

irradiation was applied to the film cross-sections. Thus, the longitudinal directions of both the SPN platelets and the cellulose II crystallites were highly oriented parallel to the film surface. Degree of orientation (Π) and Herman's orientation parameter (f) values were calculated for the cellulose II crystallites and SPN platelets in the LUC-SPN15 and LUC-SPN15D films from the 2D XRD patterns, and are listed in Table I. Both the SPN platelets and the cellulose II crystallites showed a high degree of orientation parallel to the film surface in the composite films, forming layered structures. Both SPN and cellulose II showed a higher degree of orientation in the drawn film LUC-SPN15D than in the undrawn film LUC-SPN15. These nanolayered SPN platelet structures had a positive influence on the mechanical, gas barrier, and thermal properties, as discussed later.[27]

Figure 4 shows SEM-EDX patterns for the SPN, Li-SPN, and LUC-SPN20 films. Most of the Na ions originally present in the SPN disappeared in the LUC-SPN20 film, similar to the Li-SPN film. Although the presence of Li in the composite film could not be directly detected in the SEM-EDX analysis (because of the analytical limitations), it is likely that almost all of the Na ions present in the original SPN were substituted by Li ions in the composite films. Such ion-exchange treatment of the SPN platelets—from Na^+ to Li^+—may have enhanced the formation of the nanolayered SPN platelet structures in the LUC-SPN composites. Both SPN and MTM consisted of the same elements, Na, Mg, Al, and Si, although their relative peak intensities in the EDX patterns were different between the two clays.[22] Because SPN had a relatively higher Na peak intensity in the EXD pattern, the result in Figure 4 more clearly showed that almost all Na^+ ions present in the original SPN were exchanged to Li^+ ions during the dissolution and regeneration process to prepare LUC-SPN films.

Optical, Mechanical, and Thermal Properties of Cellulose-Saponite Composite Films

Figure 5 shows the optical transmittance of the LUC and LUC-SPN nanocomposite films, as well as photograph of LUC-SPN15 film. The data for LUC-MTM composite films at 600 nm are also included in this figure for comparison.[22] With the same clay contents, the LUC-SPN composite films showed higher optical transmittances than the LUC-MTM composite films, probably because of the smaller SPM platelets and their more uniform morphology. The optical transmittance of the LUC-SPN films at 600 nm ranged from 86−88% for SPN contents of 5−15 wt %. These high optical transparencies also indicated good compatibility between the cellulose molecules and the SPN platelets, and the formation of sufficiently nanodispersed states for the SPN platelets in the composite films. The optical transmittance of the LUC-SPN20 film decreased slightly to 78%, indicating some aggregation of the SPN platelets in the composite film, due to the high SPN loading. However, the degrees of clay aggregation in the composite films

Table I. Degree of Orientation (Π) and Herman's Orientation Parameter (f) Values for Cellulose II Crystallites and SPN Platelets in the LUC-SPN15 and LUC-SPN15D Films

Sample	Crystal plane	Degree of orientation, Π (%)	Herman's orientation parameter, f
LUC-SPN15	(1 −1 0) of cellulose	82.2	0.84
LUC-SPN15D	(1 −1 0) of cellulose	84.2	0.88
LUC-SPN15	(0 0 1) of SPN	82.6	0.86
LUC-SPN15D	(0 0 1) of SPN	87.0	0.89

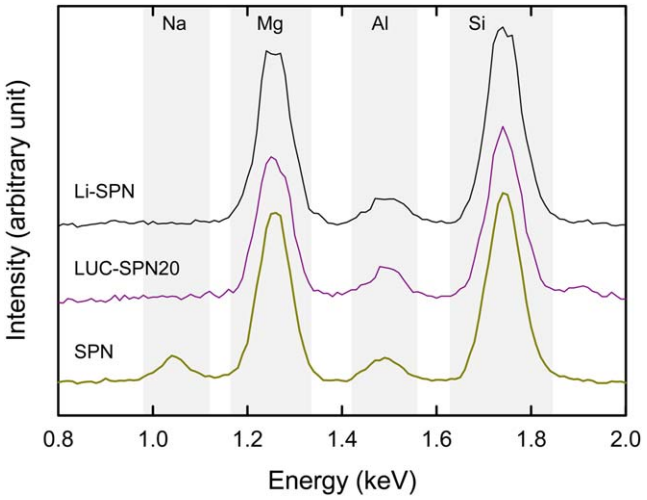

Figure 4. SEM-EDX patterns for SPN, LUC-SPN20, and Li-SPN films.

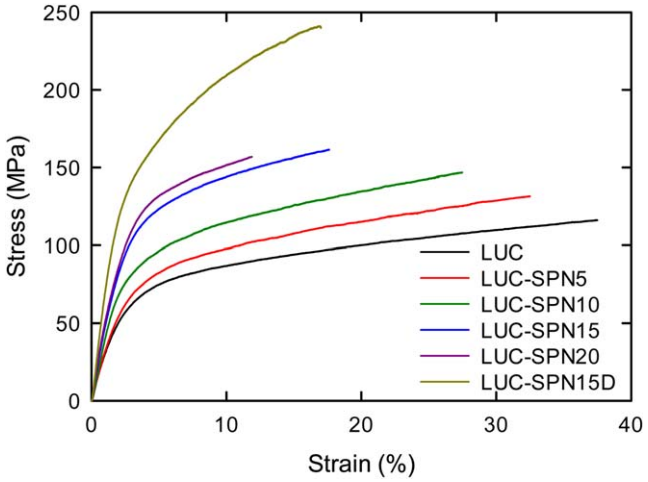

Figure 6. Stress–strain curves for LUC and LUC-SPN composite films. [Color figure can be viewed in the online issue, which is available at wileyonlinelibrary.com.]

are likely to be lower than those of LUC-MTM films because of smaller plate size of SPN.

Stress–strain curves for the LUC and LUC-SPN composite films are shown in Figure 6. The neat SPN film was too brittle to undergo tensile testing. The mechanical properties of the composite films are listed in Table II together with the data for LUC-MTM15 for comparison.[22] The Young's modulus of the LUC-SPN composite films increased from 3.4 to 5.5 GPa as the SPN content was increased from 0 to 20 wt %. The tensile strength of the LUC film was improved from 116 to 161 MPa for 15 wt % SPN contents. The tensile strength and Young's modulus of the LUC-SPN15D composite film reached 241 MPa and 7.7 GPa, respectively, when a simple drawing treatment was applied, probably due to the increase in the orientation of the cellulose II crystallites and SPN platelets in the film (Figure 3 and Table I). When the SPN content was 20 wt %, the tensile strength decreased to 157 MPa, which might have been due to some aggregation of the SPN platelets in the composite. The works of fracture for the LUC-SPN films (14–35 MJ m^{-3}) were higher than those of wood (dry yew), steel (spring), bone, and rubber (natural), which have values of 0.5, 1, 3, and 10 MJ m^{-3}, respectively; this indicated the high toughness of the LUC-SPN films.[30] The elongations at break of the LUC-SPN films were large (12–37%, depending on SPN content), indicating the good ductility of the composite films. The improvement of these mechanical properties showed that the SPN platelets were sufficiently dispersed in the cellulose matrix at the individual nanoplatelet level.[23,27] As shown in Table II, the mechanical properties of LUC-MTM15 were, in most cases, higher than those of LUC-SPN15 because of the difference in size between the two nanoclays.[22] However, the mechanical properties were clearly improved for LUC-SPN15D by drawing.

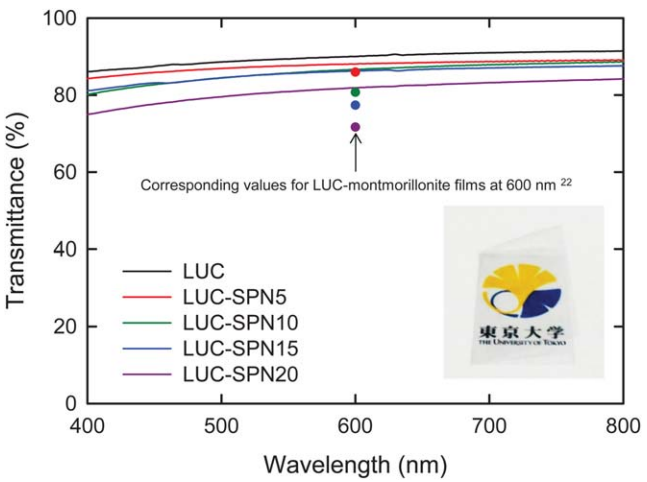

Figure 5. Visible light transmittances of LUC and LUC-SPN films. Inset shows a photograph of LUC-SPN15 film with a thickness of 30 μm. Data for LUC-MTM films[22] are included for comparison. [Color figure can be viewed in the online issue, which is available at wileyonlinelibrary.com.]

The thermal expansion behavior of the films was measured under a nitrogen atmosphere, after the films were heated at 120°C for 10 min to remove any residual moisture (Table II). The coefficient of thermal expansion of the LUC-SPN composite films decreased from 18.4 to 13.2 ppm K^{-1} as the SPN content was increased from 0 to 15 wt %, in the temperature range from 28 to 100°C. Thus, the thermal dimensional stability of the regenerated cellulose film was improved by the compositing with SPN, probably due to the presence of the intercalated nanolayered SPN platelet structures in the cellulose matrix.

Gas Barrier Properties of Cellulose-Saponite Composite Films

The oxygen transmission rates of the LUC-SPN composite films at 0% RH were less than 0.0005 mL m^{-2} day^{-1} kPa^{-1}, which was the detection limit of the instrument. This value was much lower than those of oxygen barrier films that are used in practice (such as ethylene-vinyl alcohol copolymers, poly(vinylidene schloride), and poly(vinyl alcohol)).[4] The nanolayered SPN platelet structures in the composite films likely increased the diffusion lengths for the oxygen atoms according to the tortuous-path model, resulting in the higher oxygen barrier properties.[23–27] Figure 7(A) shows the oxygen permeabilities of the LUC and LUC-SPN composite films at 50 and 75%

Table II. Mechanical and Thermal Properties of LUC and LUC-SPN Composite Films

Sample	Tensile strength (MPa)	Young's modulus (GPa)	Elongation at break (%)	Work of fracture (MJ m^{-3})	Coefficient of thermal expansion (ppm K^{-1})
LUC	116 ± 21	3.4 ± 0.4	37 ± 9	35.0 ± 2.5	18.4
LUC-SPN5	132 ± 9	3.6 ± 0.3	32 ± 6	33.5 ± 1.6	14.5
LUC-SPN10	147 ± 17	4.2 ± 0.5	27 ± 9	31.6 ± 2.8	13.9
LUC-SPN15	161 ± 9	5.2 ± 0.3	18 ± 6	22.6 ± 1.2	13.2
LUC-SPN20	157 ± 13	5.5 ± 0.6	12 ± 2	14.4 ± 0.8	13.4
LUC-SPN15D	241 ± 10	7.7 ± 0.5	17 ± 3	31.1 ± 0.9	–
LUC-MTM15[a]	187 ± 11	6.1 ± 0.8	17 ± 6	25.7 ± 2.4	11.1

[a] MTM: montmollironite.[22]

relative humidity (RH), together with some data of LUC-MTM15 for comparison.[22]

The oxygen permeability of the LUC film was 0.58 and 5.9 mL μm m^{-2} day^{-1} kPa^{-1} at 50 and 75% RH, respectively. The hydrophilic nature of the cellulose molecules resulted in a high moisture content of 10.3 wt % at 50% RH, which enhanced the dissolution and diffusion of oxygen molecules in the water absorbed on the LUC film, leading to a significant increase in the oxygen permeability.[19] On the other hand, the oxygen permeability of the LUC film decreased even at 50 and 75% RH when a composite was formed with SPN. The oxygen permeabilities of the LUC-SPN composite films under such high RH conditions were comparable with those of practical oxygen barrier films such as poly(vinylidene chloride) (0.4–5.1 mL μm m^{-2} day^{-1} kPa^{-1} at 50% RH), and were much lower than that of high density poly(ethylene) (427 mL μm m^{-2} day^{-1} kPa^{-1} at 50% RH) or poly(ethylene terephthalate) (15.6 mL μm m^{-2} day^{-1} kPa^{-1} at 50% RH).[31] Although the water vapor permeability of the LUC film clearly increased with increasing RH, it was slightly decreased by the compositing with SPN [Figure 7(B)].

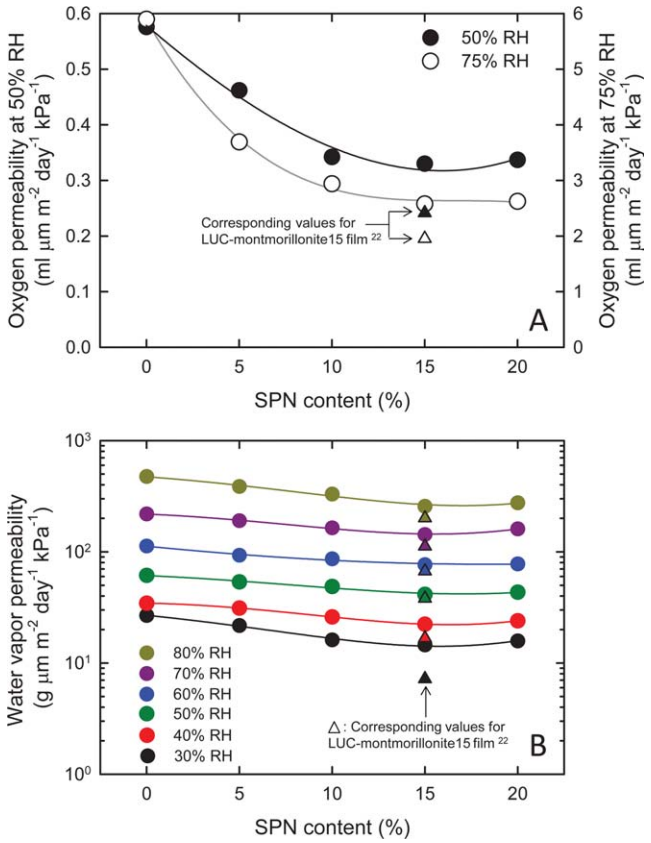

Figure 7. Gas permeabilities of LUC and LUC-SPN composite films: (A) oxygen permeability at 50% and 75% RH, and (B) water vapor permeabilities under various RH conditions. Data for LUC-MTM15 films[22] are included for comparison. [Color figure can be viewed in the online issue, which is available at wileyonlinelibrary.com.]

Some data for LUC-MTM15 were included in Figure 7(A,B) for comparison.[22] Because the average plate size of SPN is much smaller than MTM, both oxygen and water vapor permeabilities of LUC-SPN15 film were higher than those of LUC-MTM15 film, which are disadvantageous as gas-barrier films.

The LUC and LUC-SPN composite films were conditioned at 23°C and 50% RH for 2 days, and the moisture contents of the films under these conditions were measured. The moisture content of the LUC film decreased from 10.3 to 4.7 wt % when the films contained 15 wt % SPN. Furthermore, the LUC, SPN, and LUC-SPN composite films were immersed in water for 6 days to measure the water uptake under equilibrium conditions.[19] The water uptake of the LUC film decreased from 93 to 70% when the content of SPN was increased from 0 to 15 wt %. Meanwhile, no weight loss was observed for the LUC or LUC-SPN films after immersion in water for extended times, showing that the SPN particles were tightly immobilized in the cellulose matrix, probably by hydrogen bonds. In contrast, the SPN films turned to powder and dispersed in the water during the immersion treatment.

CONCLUSIONS

Transparent LUC-SPN composite films were fabricated from cellulose/LiOH/urea solutions; these films showed high mechanical strengths and Young's moduli—as well as low coefficients of thermal expansion and low oxygen permeabilities—compared with the original LUC film. The formation of sufficiently intercalated and nanolayered SPN platelet structures in the cellulose

matrix was likely responsible for the improvements in the film properties. The LUC-SPN15 composite film had especially high tensile strength and Young's modulus values (139 and 153%, respectively), greater than those of the LUC film, and the coefficient of thermal expansion and oxygen permeability at 50–75% RH decreased to 72 and 57–43%, respectively. Furthermore, the LUC-SPN composite films had large works of fracture and elongations at break; these composite films had high toughness and good ductility. The tensile strength and Young's modulus of the composite film were further improved through a simple drawing process, probably owing to improvements in the orientation of the cellulose II crystallites and SPN platelets in the composite film. Thus, these cellulose-saponite composite films are promising as high-performance packaging materials.

ACKNOWLEDGEMENTS

This study was supported by the Japan Society for the Promotion of Science (JSPS): Grant-in-Aid for Scientific Research S (21228007), and Research Fellowships for Young Scientists (24–7663).

REFERENCES

1. Ebina, T.; Mizukami, F. *Adv. Mater.* **2007**, *19*, 2450.
2. Aulin, C.; Salazar-Alvarezbc, G.; Lindström, T. *Nanoscale* **2012**, *4*, 6622.
3. Burrows, P. E.; Graff, G. L.; Gross, M. E.; Martin, P. M.; Shi, M. K.; Hall, M.; Mast, E.; Bonham, C.; Bennett, W.; Sullivan, M. B. *Displays* **2001**, *22*, 65.
4. Lange, J.; Wyser, Y. *Packag. Technol. Sci.* **2003**, *16*, 149.
5. Affinito, J. D.; Gross, M. E.; Coronado, C. A.; Graff, G. L.; Greenwell, E. N.; Martin, P. M. *Thin Solid Films* **1996**, *291*, 63.
6. Leterrier, Y. *Prog. Mater. Sci.* **2003**, *48*, 1.
7. Yu, L.; Dean, K.; Li, L. *Prog. Polym. Sci.* **2006**, *31*, 576.
8. Ohlrogge, J.; Allen, D.; Berguson, B.; DellaPenna, D.; Shachar-Hill, Y.; Stymne, S. *Science* **2009**, *324*, 1019.
9. Zhou, J.; Li, R.; Liu, S.; Li, Q.; Zhang, L. Z.; Zhang, L.; Guan, J. *J. Appl. Polym. Sci.* **2009**, *111*, 2477.
10. Fink, H. P.; Weigel, P.; Purz, H. J.; Ganster, J. *Prog. Polym. Sci.* **2001**, *26*, 1473.
11. Chae, D. W.; Kim, B. C.; Lee, W. S. *J. Appl. Polym. Sci.* **2002**, *86*, 216.
12. Zhu, S.; Wu, Y.; Chen, Q.; Yu, Z.; Wang, C.; Jin, S.; Ding, Y.; Wu, G. *Green Chem.* **2006**, *8*, 325.
13. Cai, T.; Zhang, H.; Guo, Q.; Shao, H.; Hu, X. *J. Appl. Polym. Sci.* **2010**, *115*, 1047.
14. Cai, J.; Zhang, L. *Macromol. Biosci.* **2005**, *5*, 539.
15. Yang, Q.; Qi, H.; Lue, A.; Hu, K.; Cheng, G.; Zhang, L. *Carbohydr. Polym.* **2011**, *83*, 1185.
16. Yang, Q.; Qin, X.; Zhang, L. *Cellulose* **2011**, *18*, 681.
17. Yang, Q.; Lue, A.; Qi, H.; Sun, Y.; Zhang, X.; Zhang, L. *Macromol. Biosci.* **2009**, *9*, 849.
18. Yang, Q.; Lue, A.; Zhang, L. *Compos. Sci. Technol.* **2010**, *70*, 2319.
19. Yang, Q.; Fukuzumi, H.; Saito, T.; Isogai, A.; Zhang, L. *Biomacromolecules* **2011**, *12*, 2766.
20. Yang, Q.; Fujisawa, S.; Saito, T.; Isogai, A. *Cellulose* **2012**, *19*, 695.
21. Yang Q.; Saito, T.; Isogai, A. *Cellulose* **2012**, 19, 1913.
22. Yang, Q.; Wu, C. N.; Saito, T.; Isogai, A. *Carbohydr. Polym.* **2012**, DOI 10.1016/j.carbpol.2012.10.044.
23. Walther, A.; Bjurhager, I.; Malho, J. M.; Pere, J.; Ruokolainen, J.; Berglund, L.A.; Ikkala, O. *Nano Lett.* **2010**, *10*, 2742.
24. Wang, J.; Cheng, Q.; Tang, Z. *Chem. Soc. Rev.* **2012**, *41*, 1111.
25. Wu, C. N.; Saito, T.; Fujisawa, S.; Fukuzumi, H.; Isogai, A. *Biomacromolecules* **2012**, 13, 1927.
26. Paul, D. R.; Robeson, L. M. *Polymer* **2008**, *49*, 3187.
27. Liu, A.; Walther, A.; Ikkala, O.; Belova, L.; Berglund, L. A. *Biomacromolecules* **2011**, *12*, 633.
28. Sehaqui, H.; Mushi, N.; Morimune, S.; Salajkova, M.; Nishino, T.; Berglund, L. A. *ACS Appl. Mater. Inter.* **2012**, *4*, 1043.
29. Bonderer, L. J.; Studart, A. R.; Gauckler, L. *J. Science* **2008**, *319*, 1069.
30. Sehaqui, H.; Zhou, Q.; Berglund, L.A. *Soft Matter* **2011**, *7*, 7342.
31. Miller, K.; Krochta, J. *Trends Food Sci. Tech.* **1997**, *8*, 228.